Monthly Notices
of the
ROYAL ASTRONOMICAL SOCIETY

Mon. Not. R. Astron. Soc. **419,** 452–464 (2012) doi:10.1111/j.1365-2966.2011.19711.x

Evolutionary models for double helium white dwarf mergers and the formation of helium-rich hot subdwarfs

Xianfei Zhang[1]★ and C. Simon Jeffery[1,2]★

[1]*Armagh Observatory, College Hill, Armagh BT61 9DG*
[2]*School of Physics, Trinity College Dublin, Dublin 2, Ireland*

Accepted 2011 August 26. Received 2011 August 26; in original form 2011 July 24

ABSTRACT

Recent surveys have demonstrated the existence of several short-period binary systems containing two white dwarfs. Following orbital decay by gravitational-wave radiation, such binaries are expected to merge at a rate of two or three per thousand years per galaxy. The consequences of such a merger depend on the individual white dwarf masses, but are believed to include helium-rich subdwarfs, R CrB stars, extreme helium stars and also AM CVn systems and possibly Type Ia supernovae.

Whilst the hydrodynamics of the merger process remains difficult to compute, it is possible to compute the evolution of a double white dwarf merger following the destruction of one component. In this paper, we describe the evolution following the merger of two helium white dwarfs. We examine three sets of assumptions concerning the distribution of debris material between a disc and a corona.

Our results demonstrate that a model comprising both fast accretion to form a (hot) corona *and* slow accretion from a (cold) debris disc can reproduce the observed distribution of helium-rich subdwarfs in terms of their surface temperatures, gravities, nitrogen and carbon abundances.

Key words: stars: abundances – binaries: close – stars: evolution – stars: peculiar – subdwarfs – white dwarfs.

1 INTRODUCTION

It is generally accepted that about 99 per cent of stars end their lives as white dwarfs (WDs). The majority of these are helium white dwarfs with mass in the range 0.17–0.45 $M_{\odot}$. Most helium white dwarfs are the result of binary star evolution; such stars lose almost all their outer envelopes without reaching the asymptotic giant branch or without ever igniting helium, and then cool to become a white dwarf. Without this channel, an isolated star with low mass would take more than a Hubble time to evolve into a white dwarf configuration. Rebassa-Mansergas et al. (2011) and Brown et al. (2011) demonstrate that a large number of low-mass white dwarfs are found in binary systems, which supports binary interaction as the dominant channel for the formation of low-mass white dwarfs at the current epoch. According to this mechanism, a significant number of binaries containing *two* helium white dwarfs are expected to exist in the Galaxy. In a survey of extremely low-mass white dwarfs, 12 very short-period white dwarf binary systems have been found, of which three will merge due to gravitational wave radiation in less than 500 Myr (Kilic et al. 2010, 2011). The most likely products of the merger of a binary comprising two helium white dwarfs are extremely helium-rich stars and helium-rich hot subdwarfs (Saio & Jeffery 2000; Han et al. 2002, 2003). A few tens of helium-rich hot subdwarfs have been found in the Galaxy, of which several have been analysed for abundances (Stroeer et al. 2007; Naslim et al. 2010). These are important candidates for understanding helium white dwarf (HeWD) mergers.

Hot subdwarfs are traditionally classified into three types by their spectra (Drilling et al. 2003): subdwarf B (sdB), with a surface effective temperature $T_{\rm eff}$ in the range 20 000–40 000 K and H-Balmer absorption lines wider than in normal B stars; subdwarf O (sdO), with $T_{\rm eff}$ ranging from 40 000–80 000 K with strong He absorption lines; and subdwarf OB (sdOB), a transition between O and B (Moehler et al. 1990; Heber 2009). These objects are located below the upper main sequence on a Hertzsprung–Russell (HR) diagram, and are also known as extreme horizontal branch stars. This is based on the understanding that they are core He-burning stars with extremely thin hydrogen envelopes ($<0.02\,M_{\odot}$). Most, but not all, sdB stars have He II lines that are very weak for their colour. Spectroscopically they form a relatively homogeneous class, whereas a larger variety of spectra is observed amongst sdO stars (Moehler et al. 1990), which display He II, 4686-Å and sometimes other He II lines, and in which Balmer lines may occasionally be

★E-mail: xiz@arm.ac.uk; csj@arm.ac.uk

absent. They are frequently subdivided according to the dominant spectral features into H-strong (sdO) and He-strong-lined (He-sdO). In contrast, helium-rich sdB (He-sdB) stars are rare. The class sdOB describing sdB-like spectra with weak He II is now often subsumed under the sdB class. In addition, the spectra of He-sdB and He-sdO stars can be grouped into carbon-strong-lined and nitrogen-strong-lined (Jeffery et al. 1997; Drilling et al. 2003; Stroeer et al. 2007).

Although the sdB stars are nearly naked helium stars, the majority retain a thin veneer of hydrogen ($\approx 0.02\,M_\odot$). With radiative envelopes and high surface gravity, whatever helium there is sinks below the surface and makes the majority appear to be quite deficient in helium. Diffusion theory, which includes radiative forces acting on ions, explains this well (Heber et al. 1986). The existence within the PG and other surveys of a fraction (10 per cent: Green, Schmidt & Liebert 1986) of 'helium-rich' sdB and sdO stars therefore poses a major challenge. Han et al. (2002, 2003) and Han (2008) have argued that HeWD mergers can explain the formation of apparently single sdB stars, but did not distinguish between the formation of H-rich and He-rich subdwarfs. Formation channels that might produce clearly helium-rich subdwarfs include HeWD mergers, as computed by Saio & Jeffery (2000), late core-helium ignition in a post-giant helium star (the 'hot flasher': Moehler et al. (2007); Miller Bertolami et al. (2008)) and the merger of a post-sdB star (a composite CO/He white dwarf) with a helium white dwarf (Justham, Podsiadlowski & Han 2011). One unexplained piece of evidence is the observation that He-rich hot subdwarfs may be divided into two groups according to whether their surfaces are nitrogen-rich or carbon-rich (Jeffery et al. 1997; Stroeer et al. 2007). Nitrogen-rich subdwarfs are simply explained by CNO-process hydrogen burning; all original carbon and oxygen is converted to nitrogen at the same time as the dominant helium is produced (Saio & Jeffery 2000). Carbon-rich subdwarfs are harder to explain since 3α-processed material must be exposed at the surface, possibly by dredge-up after helium ignition but before the star becomes a hot subdwarf. A judicious choice of mixing physics has yielded carbon-rich surfaces in some of the above models, but it is not yet clear whether it is possible to explain both carbon- and nitrogen-rich groups within the same model, or under what conditions flash- and opacity-driven convection can combine to bring carbon to the surface.

In this paper, we set up three possible merger models for helium + helium white dwarf binaries. We calculate the evolution following that merger and compare the results with recent observational data for helium-rich subdwarfs.

2 A BRIEF VIEW OF THE MERGER PROCESS

There are two key requirements for a close binary white dwarf to merge and form a single star. The first principle is gravitational radiation. Due to gravitational radiation, a double white dwarf system loses orbital angular momentum $J_{\rm orb}$ and causes the binary separation a to decay until the larger star fills its Roche lobe. The rate of loss of orbital angular momentum (Landau & Lifshitz 1962) is expressed as

$$\frac{\dot{J}_{\rm orb}}{J_{\rm orb}} = -8.3\times10^{-10}\times\left(\frac{m_1}{M_\odot}\right)\left(\frac{m_2}{M_\odot}\right)\left(\frac{m_1+m_2}{M_\odot}\right)\times\left(\frac{a}{R_\odot}\right)^{-4}\ {\rm yr}^{-1}, \quad (1)$$

where m_1 and m_2 are the masses of stars in the binary.

The second requirement is the mass ratio q. If

$$q \equiv m_1/m_2 \geq q_{\rm crit} \equiv \frac{5}{6} + \frac{\zeta(m_2)}{2}, \quad (2)$$

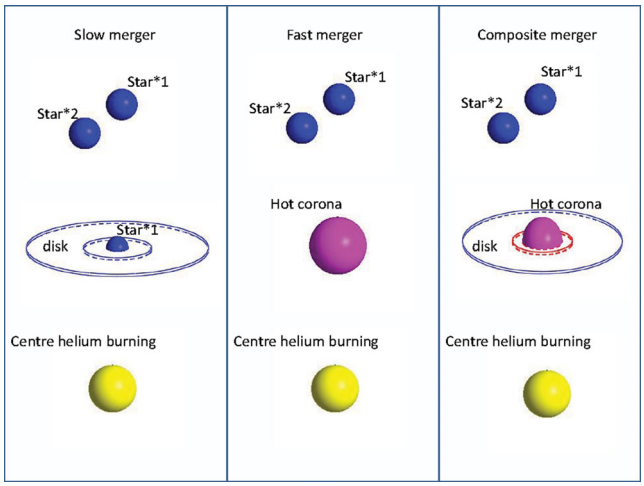

Figure 1. Schematic of three possible ways in which two helium white dwarfs might merge.

where $\zeta(m_2) \equiv {\rm d}\ln r/{\rm d}\ln m$ is obtained from the white dwarf mass–radius relation, the radius of the larger (less massive) white dwarf will increase more quickly than the separation due to the transfer of angular momentum, leading to unstable (runaway) mass transfer on a dynamical time-scale (a few seconds). If $q \leq q_{\rm crit}$, stable mass transfer will occur, possibly leading to the formation of an AM CVn binary: an ultrashort binary system containing two helium white dwarfs.

Hydrodynamical simulations of the merger of two low-mass white dwarfs suggest that a number of phases occur. Following the complete tidal disruption of the lower mass component (secondary), its material may be redistributed around the more massive component (primary) in (a) a cold Keplerian debris disc and (b) a hot spherical corona. From a schematic point of view, there are three possible ways to combine these processes, which we shall call the slow (or cold) merger, the fast (or hot) merger and the composite (fast + slow) merger model (Fig. 1).

A disc allows cold mass to migrate towards its centre, from where it can be accreted slowly on to the primary surface, while angular momentum is dissipated towards the disc circumference (Lynden-Bell & Pringle 1974). The slow merger model assumes that the secondary transfers its entire mass to form a disc around the primary within a few minutes, after which mass accretes from the disc to the primary at a rate comparable to the Eddington accretion rate. This process could last for several million years (Tutukov & Yungelson 1979; Iben & Tutukov 1984; Nomoto & Iben 1985; Mochkovitch & Livio 1989, 1990; Saio & Nomoto 1998; Saio & Jeffery 2000, 2002).

The fast merger model assumes that the less massive white dwarf quickly transfers its entire mass to the companion surface directly, where heating to 10^8 K makes the material expand to form a hot corona within a few minutes (Benz et al. 1990; Guerrero, García-Berro & Isern 2004).

The composite merger model includes both processes, in which about 30 $\sim$ 50 percent of the mass of the secondary forms a hot corona around the survivor, while the rest of the destroyed white dwarf forms a Keplerian disc (Yoon, Podsiadlowski & Rosswog 2007; Lorén-Aguilar, Isern & García-Berro 2009).

In both the slow and fast + slow modes, the accretion rate from the Keplerian disc has been assumed to be about half the Eddington

rate, i.e. $10^{-5}\,M_\odot\,yr^{-1}$, although higher rates could be realized in practice.

3 METHODS

To calculate the evolution of the WD model stars as well as the further evolution of the collision product, we use the stellar evolution code Modules for Experiments in Stellar Astrophysics (MESA: Paxton et al. 2011). By using adaptive mesh refinement and sophisticated time-step controls, MESA solves the fully coupled structure and composition equations simultaneously. We set the ratio of mixing length to local pressure scale height, $\alpha = l/H_p$, to 2.0. The opacity tables for various metallicities are compiled by Iglesias & Rogers (1996) and Alexander & Ferguson (1994).

As Nelemans et al. (2000) shows, the most common helium white dwarf binaries descend from systems in which both stars have $M \leq 2.3\,M_\odot$. However, for our experiments, it is difficult to control the final mass of the helium white dwarf we require from a full binary-star evolution calculation. Thus, an artificial method is adopted. We start with a zero-age main-sequence star of mass $2.0\,M_\odot$ and evolve it until the helium core reaches the required mass. Then all the envelope is removed by hand to produce a naked helium core, essentially a pre-WD model. These models cannot ignite centre helium burning and evolve straight to the white dwarf sequence, ending up with a luminosity of $\log L/L_\odot = -2$.

Starting with this helium white dwarf model, material is accreted at the surface until the desired mass is achieved. The thermal structure of the outer layers is governed by the accretion rate. Nucleosynthesis is included in the calculation. Once steady helium burning is established, evolution is followed until the star has evolved to become a white dwarf.

4 NUMERICAL EXPERIMENTS

As introduced above, we consider three possible scenarios for a He + He merger. For each scenario, we have calculated four model sequences, starting with nearly equal-mass pairs, i.e. $0.25 + 0.25, 0.30 + 0.30, 0.35 + 0.35$ and $0.40 + 0.40\,M_\odot$. The accretion of helium-rich material is modelled in three ways. The composition of the accreted material is assumed to be $Y = 0.98$, $Z = 0.02$, where the detail metal abundance distribution is obtained from the average abundance of different mass WD models, as shown in Fig. 2. The merger scenario shows a less massive white dwarf being disrupted because it fills its Roche lobe before the more massive white dwarf. In the present experiments we have chosen the secondary to be of equal mass to the primary; this is the upper extreme. Physically, the secondary mass would have to be marginally smaller than that of the primary. The lower extreme would be the minimum mass for dynamically unstable mass transfer, but that value is less well-defined. Investigating several masses between these extrema for every scenario would have been costly, and not necessarily any more informative.

Thus, the composition of accreted material is, by mass fraction, ^{12}C: 6.00×10^{-5}; ^{14}N: 1.27×10^{-2}; ^{16}O: 1.64×10^{-3}; ^{20}Ne: 1.88×10^{-3}; ^{24}Mg: 3.68×10^{-3}.

For this numerical experiment, we assume that a fast merger phase has a constant accretion rate of $10^4\,M_\odot\,yr^{-1}$, which makes the merger process finish within a few minutes. For the slow merger we adopt a constant accretion rate of $10^{-5}\,M_\odot\,yr^{-1}$. For the composite merger, we assume that all models start with fast accretion, i.e. $10^4\,M_\odot\,yr^{-1}$, leaving a $0.1\,M_\odot$ disc for slow accretion at $10^{-5}\,M_\odot\,yr^{-1}$.

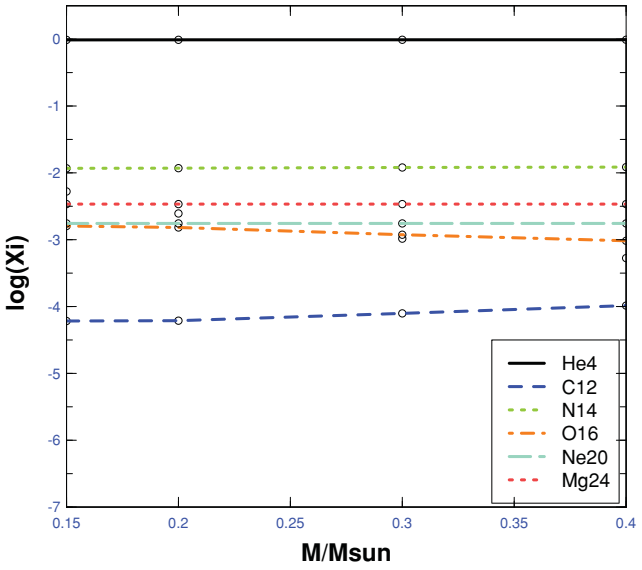

Figure 2. The average composition of helium white dwarf models as a function of mass, showing ^{12}C, ^{14}N, ^{16}O, ^{20}Ne, ^{24}Mg (colour in online version).

4.1 Slow merger

The slow merger model has previously been discussed by Saio & Jeffery (2000) for He + He mergers and also by Saio & Jeffery (2002) for CO + He mergers. Here we use similar assumptions and methods, although the computational code is completely independent. The results are shown below.

Figs 3 and 4 illustrate the internal evolution and the final chemical and thermal structure of a $0.4\text{-}M_\odot$ cool white dwarf accreting material to reach a final mass of $0.8\,M_\odot$. The 3α and other alpha capture reactions (on to C, N and O elements) are ignited at the surface of primary when the total mass has increased to $0.44\,M_\odot$

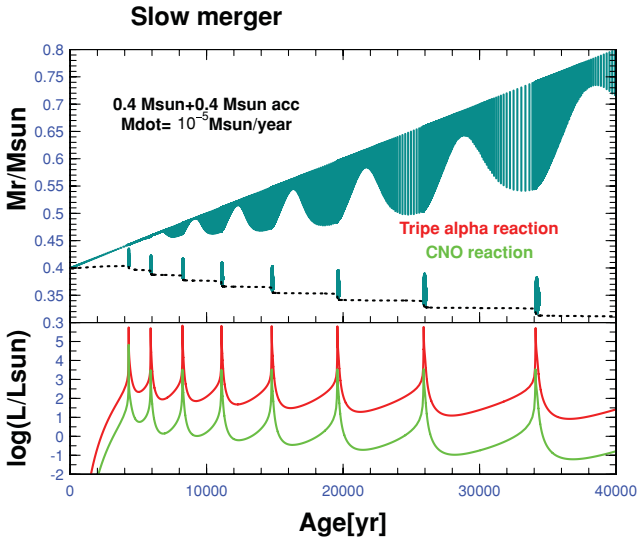

Figure 3. Internal evolution during a slow merger between two $0.4\text{-}M_\odot$ white dwarfs. Top panel: location of convective regions during accretion of helium. The accretion rate is $10^{-5}\,M_\odot\,yr^{-1}$ during the whole process. The zones are only shown for each time-step in the model sequence; the gaps between models are longer than they are during shell flashes. Bottom panel: energy generated from 3α (dark grey, red online) and other alpha capture (light grey, green online) reactions on to C, N and O elements.

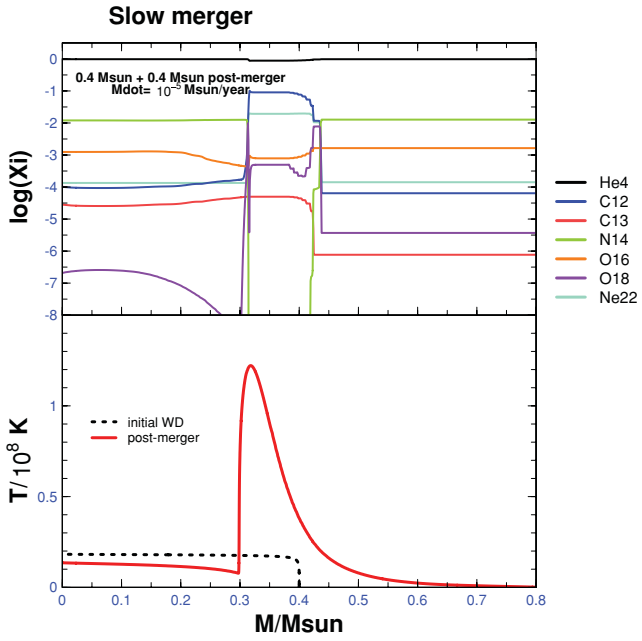

Figure 4. The internal temperature and abundance structure following a slow merger between two 0.4-$M_\odot$ white dwarfs. The top panel shows the composition profile just after completion of the merger. The bottom panel shows the temperature profiles of the initial 0.4-$M_\odot$ helium white dwarf (dotted line) and the 0.8-$M_\odot$ merged star just after completion of the merger (solid line).

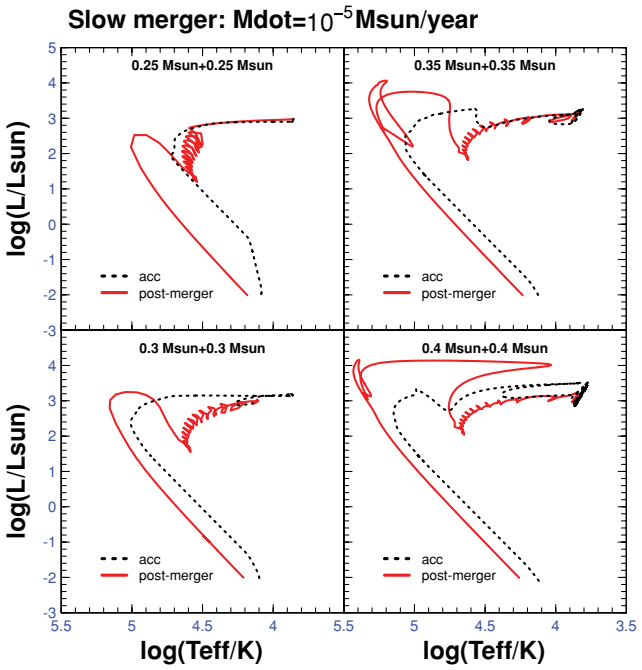

Figure 5. The HR diagram of the slow merger model. The evolutionary tracks start with an accreting white dwarf of 0.25, 0.30, 0.35 and 0.4 $M_\odot$. The accretion was stopped when the total mass became 0.5, 0.6, 0.7 and 0.8 $M_\odot$ respectively (dotted line). The solid line shows the evolutionary tracks following the merger.

(Fig. 3). Subsequently, the helium-burning flame moves inwards in a series of shell flashes. Each peak of luminosity is about 10^6 $L_\odot$ and the energy released causes the radius to increase, leading the star to evolve to become a yellow giant. About eight flashes after 3α ignition, accretion stops ($M = 0.8$ $M_\odot$) and the merged star attains a radius of $\approx$18 $R_\odot$.

Fig. 4 shows detail of the temperature profile of the initial helium white dwarf (before accretion) and of the post-merger star immediately after accretion is completed. A detailed abundance profile of the post-merger star is also shown, in which we can see that carbon is produced by helium-shell burning and that nitrogen is destroyed by the 3α reaction.

After accretion is completed, the helium-burning shell continues to move inwards in a series of repeating shell flashes (cf. Saio & Nomoto 1998; Saio & Jeffery 2000). During the quiescent phase between flashes, the helium-burning shell heats the cool degenerate material beneath it until it is sufficiently hot to burn. The strength of each shell flash decreases as the shell moves inwards and also causes the total radius of the star to decrease and the effective temperature to increase. After $\approx$15–20 flashes or about 5×10^5 yr the helium-burning shell reaches the centre of the star, while the star itself contracts to a radius of $\approx$0.2 $R_\odot$. Fig. 5 shows the evolutionary tracks for all four models. The dashed line shows the accretion phase and the solid line the post-merger track. Once the flame reaches the centre of the star, i.e. the end of the loops on the HR diagram, core burning is established. Since the inward shell-flash phase consumes only a fraction of the available helium in the core, the next phases of evolution strongly resemble standard extended horizontal-branch evolution (Saio & Jeffery 2000). Thus, after core helium exhaustion, a helium-burning shell forms and moves outward (in mass), causing an increase in luminosity. After shell exhaustion, the star contracts to form a hybrid CO/He white dwarf.

The location of convective regions during the accretion and immediate post-merger phases of a $0.4 + 0.4$ $M_\odot$ merger are shown in Fig. 6. The flash-driven convection zones in the interior occur during helium flashes and move inwards along with the helium-burning shell, which is located at the base of the convection zone. The surface convection zone reflects the effective temperature at the surface. As the figure shows, even if the helium-burning flame produces a lot of carbon the surface convection zone does not extend to reach this carbon-rich region and cannot dredge fresh carbon up to the surface. Thus in this model the surface abundance remains the same as that of the donor white dwarf.

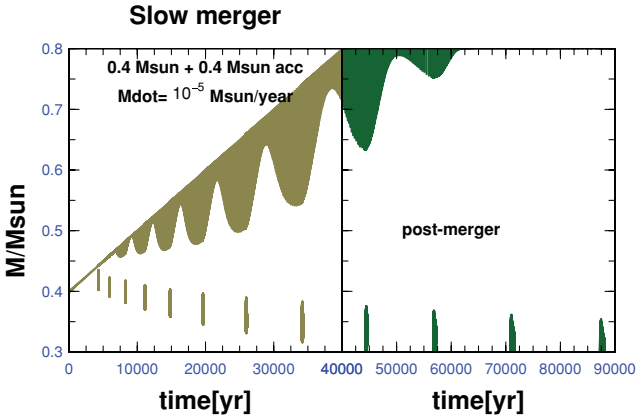

Figure 6. Left: the location of convective regions during accretion of helium by a 0.4-$M_\odot$ helium white dwarf to 0.8 $M_\odot$. The accretion rate is 10^{-5} $M_\odot$ yr^{-1} during the whole process. The zones are only shown for each time-step in the model sequence; the gaps between models are longer than they are during shell flashes. Right: the location of convective regions post-merger.

Pairs with lower masses shows a similar behaviour. However, less massive stars undergo fewer shell flashes, which take more time to reach the centre of the star. For all slow merger models, the abundance at the surface is as the same as that of the secondary white dwarf.

4.2 Fast merger

For the fast merger model, we arbitrarily assumed an accretion rate of $10^4\,M_\odot\,yr^{-1}$ so that it takes only a few minutes for the material to be accreted. In a real merger this would be a violent and highly turbulent process, with considerable associated heating. We have here made the assumption of quasi-hydrostatic equilibrium throughout the fast accretion phase, so there is no dynamical heating of the accreted material. Instead we rely on the much more dominant nuclear heating to determine the post-accretion structure. Fig. 7 shows various properties as a 0.4-$M_\odot$ cool white dwarf accretes mass to reach a final mass of $0.8\,M_\odot$. The 3α and other alpha capture reactions are ignited at the surface of the primary almost immediately. Because of the high accretion rate, nuclear ignition is different from the slow merger case; there is no runaway helium flash and burning is stable. Most of the energy released during this process goes into heating the corona, which expands to $\sim 0.07\,R_\odot$.

Fig. 8 shows more details of the temperature profile of the initial helium white dwarf before accretion and of the post-merger star at the end of the accretion process. After the merger, the helium-burning shell reaches a peak temperature of about 4×10^8 K. A detailed abundance profile of the post-merger star is also shown in Fig. 8, where it can be seen that (a) carbon is produced by helium burning and partially mixed outward and (b) nitrogen is destroyed by the alpha capture. An interesting thing is that at such a high temperature the destruction of ^{14}N by the $^{14}N(\alpha,\gamma)^{18}O$ reaction becomes more efficient than it is at low temperature, as Warner (1967) and Clayton et al. (2007) indicated. This reaction very quickly makes ^{18}O the most abundant of the CNO isotopes. This situation lasts until ^{18}O begins α-capturing as the temperature continues to increase,

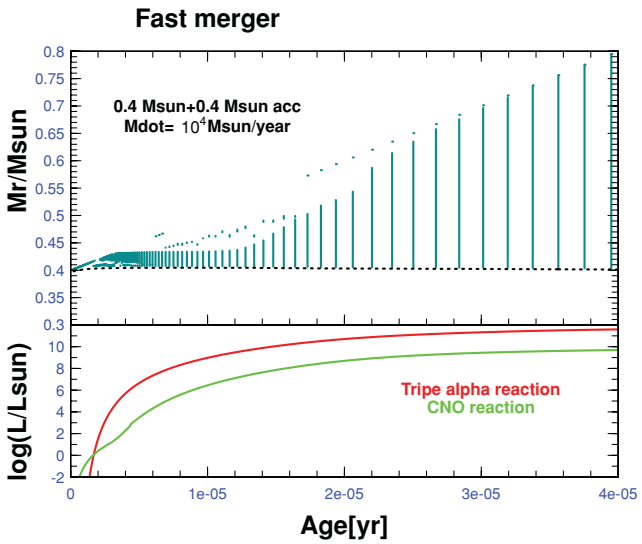

Figure 7. Convection zones and energy released during a fast merger. Top panel: the location of convective regions during accretion of helium by a 0.4-$M_\odot$ helium white dwarf. The accretion rate is $10^4\,M_\odot\,yr^{-1}$ during the whole process. The zones are only shown for each time-step in the model sequence. Bottom panel: the energy generated from 3α and other alpha capture (green) reactions on to C, N and O elements.

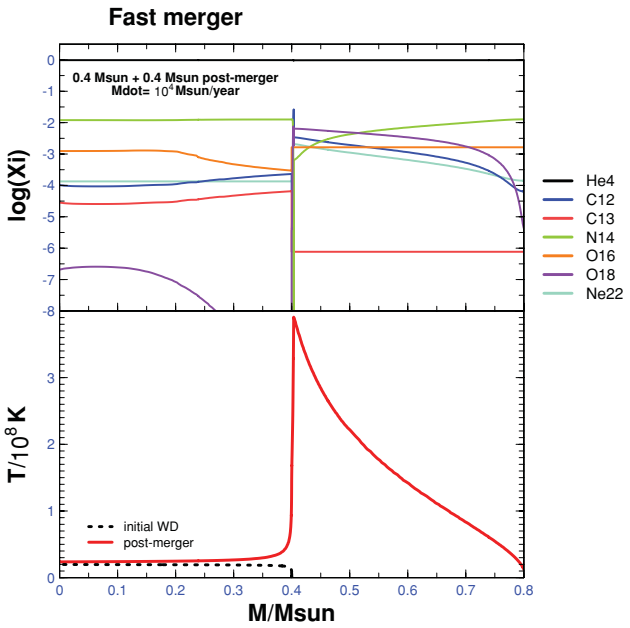

Figure 8. The temperature and abundance profile during a fast merger. Top panel: the abundance profile at the time just before the end of the merger, i.e. as an accreting 0.4-$M_\odot$ helium white dwarf reaches $0.8\,M_\odot$. Bottom panel: the temperature profile of the initial 0.4-$M_\odot$ helium white dwarf (dotted) and the completed 0.8-$M_\odot$ merger (solid).

which produces ^{22}Ne. Thus, the abundance of ^{18}O is very sensitive to the physical conditions, i.e. temperature, density and composition. Obviously, if the high temperature persists for a long period, ^{22}Ne will be the most abundant of the CNO isotopes. In the fast merger, the convection speed is around $7\,cm\,s^{-1}$, giving a convective turnover time of $\approx$20 yr, which is sufficiently short compared with the evolution time following the merger. As Fig. 9 shows, the whole envelope is fully convective at the end of the merging process and thus the hot corona is completely mixed and shows a high surface abundance of ^{12}C, ^{18}O and ^{22}Ne.

After the merger, the increasing nuclear luminosity forces the star to expand; the radius becomes about 50 $R_\odot$ within 10^4 yr (see

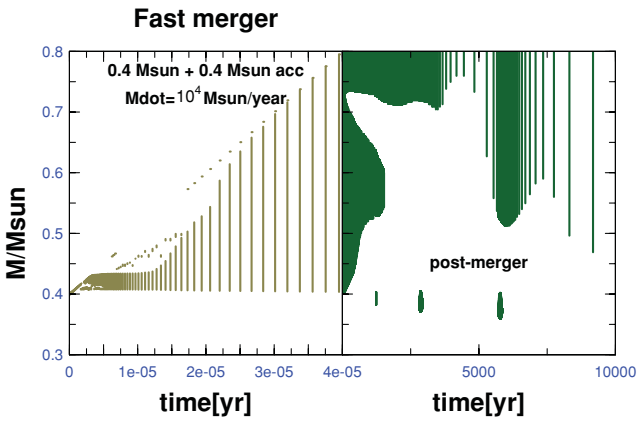

Figure 9. Left: the location of convective regions during accretion of helium by a 0.4-$M_\odot$ helium white dwarf to $0.8\,M_\odot$. The accretion rate is $10^4\,M_\odot\,yr^{-1}$ during the whole process. The zone are only shown for each time-step in the model sequence; the gaps between models are longer than they are during shell flashes. Right: the location of convective regions post-merger.

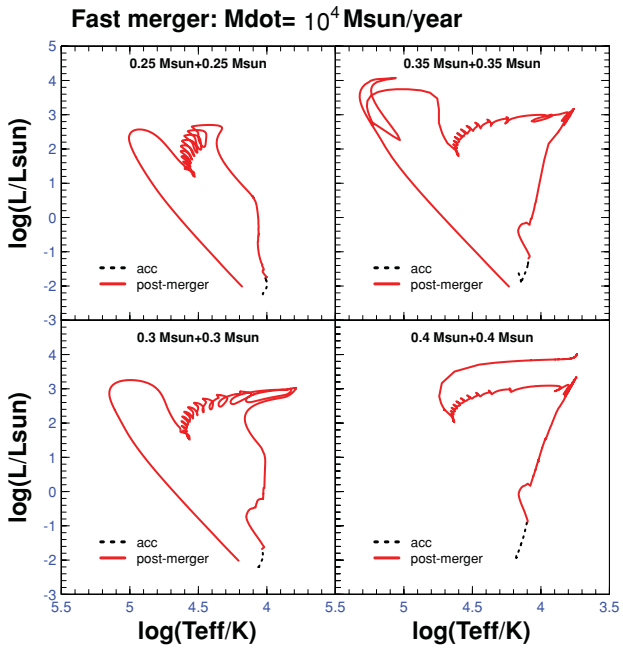

Figure 10. Evolution tracks for fast merger models. The tracks show the initial models for white dwarfs with inital masses 0.25, 0.30, 0.35 and 0.4 $M_\odot$ accreting to reach final masses 0.5, 0.6, 0.7 and 0.8 $M_\odot$ respectively (dotted line). The solid lines show how the evolution following the merger is completed.

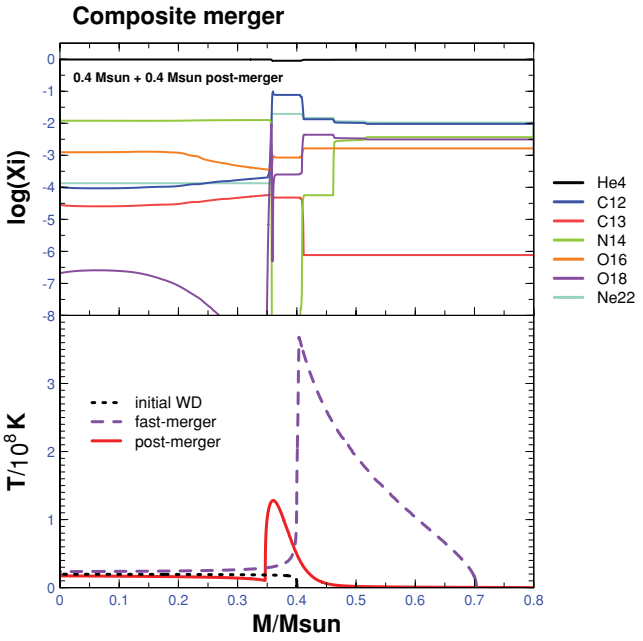

Figure 11. The temperature and abundance profile during a composite merger. Top panel: the abundance profile just after completion of the merger, i.e. for a 0.4-$M_\odot$ helium white dwarf accreting helium to become a 0.8-$M_\odot$ star. Bottom panel: the temperature profile of the initial 0.4-$M_\odot$ helium white dwarf (dotted line), the hot coronal object at the end of the fast merger phase (dashed) and the final 0.8-$M_\odot$ merged star (solid).

Fig. 10). Subsequently, the helium-burning shell moves inwards with a series of flashes. After ≈20 flashes, or about 7×10^5 yr, the helium-burning flame reaches the centre of the star. At the same time, the overall radius of the star is reduced to ≈0.2 $R_\odot$ and the effective temperature increases gradually. Once the flame reaches the centre of the star, i.e. at the end of the loops on the L–$T_{\rm eff}$ diagram, central helium-core burning is established. The following evolution behaves exactly as a helium star would (Saio & Jeffery 2000), as well as the slow merger models shown above. After core helium exhaustion a helium-burning shell develops, leading to a period of expansion and higher luminosity followed by contraction to the white dwarf cooling branch.

For the $0.25 + 0.25\,M_\odot$ model, the stored thermal energy is not enough to force expansion to the giant branch; maximum expansion only reaches a temperature and luminosity similar to that of a blue horizontal branch star. Higher mass pairs, i.e. $0.3 + 0.3\,M_\odot$ and $0.35 + 0.35\,M_\odot$, behave similarly to the $0.4 + 0.4\,M_\odot$ models shown. However, these stars undergo fewer shell-flash cycles and it takes more time for inward-burning flashes to reach the centre of star. For all of the fast merger models the surface composition is rich in ^{12}C, ^{18}O and ^{22}Ne, but there is almost no ^{14}N.

4.3 Composite merger

The composite merger model considers two processes. First, more than half the mass of the secondary is rapidly accreted by the primary to form a hot corona, as in the fast merger model. Secondly, the remaining material from the secondary is accreted on to the hot corona, as in the slow merger model.

During fast accretion, the star expands as in the fast merger. During slow accretion, the inward-burning shell flashes cause the star to execute blue loops in the L–$T_{\rm eff}$ diagram, but continuing accretion maintains the star as a cool giant. After slow accretion terminates, the nuclear burning temperature is reduced and the temperature profile starts to resemble that in the slow merger model. Subsequently, the helium-burning flame propagates inwards as in both the slow and fast merger models.

Taking the $0.4 + 0.4\,M_\odot$ model as an example (Fig. 11), the first fast-accretion stage takes around 16 min to form a hot corona with a radius 0.06 $R_\odot$ (recall that the radius of a 0.4-$M_\odot$ white dwarf is approximately 0.01 $R_\odot$). During the stable helium-burning phase, almost complete envelope convection brings material rich in ^{12}C, ^{18}O and ^{22}Ne ashes close to the surface (Fig. 13).

During the second slow-accretion phase the helium-burning shell still heats the corona, forcing it to continue expanding. At the beginning of this process the corona/envelope is fully convective and the helium-burning makes the corona rich in ^{12}C, ^{18}O and ^{22}Ne. The surface abundances ^{12}C, ^{18}O, ^{22}Ne and ^{14}N subsequently develop a dynamic balance because of (i) the nitrogen-rich materials continually being accreted into the corona from the disc and (ii) the conversion of ^{18}O to ^{22}Ne through α-capture because temperatures are still high. During this process, helium-flash cycles commence. The strength of each flash peak increases gradually. As the helium flame moves inwards, the star initially expands to ≈32 $R_\odot$ within 4×10^3 yr and then contracts away from the giant branch during the remainder of the slow-accretion phase (Fig. 12).

In subsequent evolution the 0.8-$M_\odot$ composite model behaves similarly to the slow merger models, as shown in Fig. 13. Thus, there follow about 20 helium flashes in 6×10^5 yr, each subsequent flash decreasing in intensity until the flame reaches the centre of the star, i.e. the end of the loops on the HR diagram. After this, a standard core-helium-burning phase is established, followed by a normal helium-shell-burning phase, leading to higher luminosity and finally cooling to the white dwarf sequence.

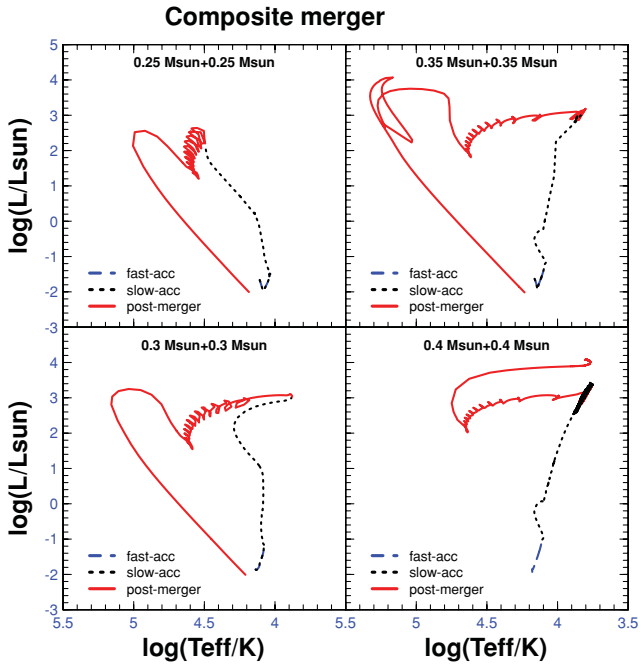

Figure 12. Evolution tracks for composite merger models. The tracks show the initial models for white dwarfs with inital masses 0.25, 0.30, 0.35 and 0.4 $M_\odot$ accreting to reach final masses 0.5, 0.6, 0.7 and 0.8 $M_\odot$ respectively (dotted line). The solid line shows the evolutionary tracks following the merger.

A significant feature of this model is seen in the central section of Fig. 13. At the end of fast accretion and the beginning of slow accretion, flash-driven convection mixes ^{12}C throughout the 0.3-$M_\odot$ envelope. Although this material is subsequently buried by C-poor material, the deep opacity-driven convection that follows

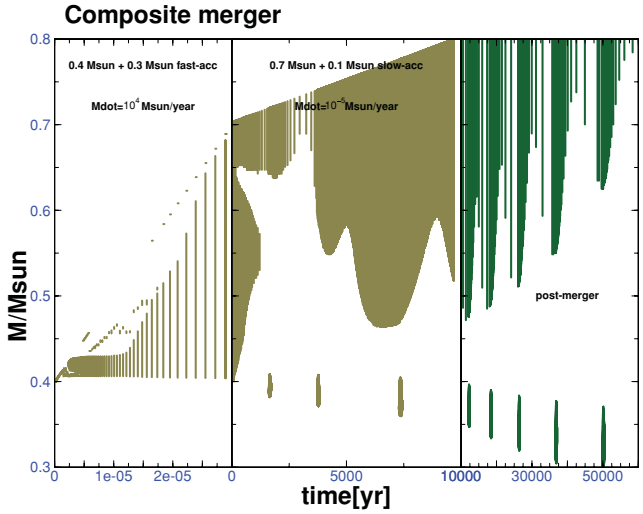

Figure 13. Left: the location of convective regions during fast accretion of helium by a 0.4-$M_\odot$ helium white dwarf to 0.7 $M_\odot$. The fast accretion rate is 10^4 $M_\odot$ yr^{-1}. The zones are only shown for each time-step in the model sequence; the time-steps between models are longer than they are during shell flashes. Middle: the location of convective regions during the slow accretion of helium to final mass 0.8 $M_\odot$. The slow accretion rate is 10^{-5} $M_\odot$ yr^{-1}. Right: the location of convective regions during the post-merger evolution of the 0.8-$M_\odot$ product.

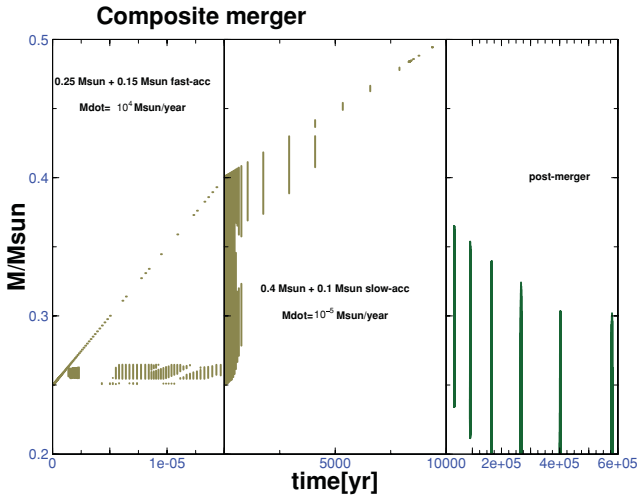

Figure 14. Left: the location of convective regions during fast accretion of helium by a 0.25-$M_\odot$ helium white dwarf to 0.4 $M_\odot$. The fast accretion rate is 10^4 $M_\odot$ yr^{-1}. The zones are only shown for each time-step in the model sequence; the time-steps between models are longer than they are during shell flashes. Middle: the location of convective regions during the slow accretion of helium to the final mass 0.5 $M_\odot$. The slow accretion rate is 10^{-5} $M_\odot$ yr^{-1}. Right: the location of convective regions during the post-merger evolution of the 0.5-$M_\odot$ product.

each shell-pulse dredges carbon-rich material to the new surface, so that the final product after slow accretion terminates is rich in ^{12}C and ^{22}Ne.

Because convection behaviour is different in the slow merger and fast merger cases, the behaviour of the composite model is even more complex. For the 0.25+0.25 $M_\odot$ and 0.3+0.3 $M_\odot$ cases, the corona/envelope is fully convective at the transitions between fast and slow phases, as shown in Fig. 14. During the subsequent slow-accretion phase there are no helium-shell flashes and so no flash-driven convection zones. Moreover, the surface is relatively hot, so the surface convection zone disappears completely. Consequently, at the end of slow accretion the surface composition of the model is determined entirely by the accreted material, which is the same as the second white dwarf. In our present calculations, we find that the composite model for a 0.35+0.35 $M_\odot$ merger is similar to that of the 0.4+0.4 $M_\odot$ case, with a surface relatively rich in ^{12}C and ^{22}Ne.

5 COMPARISON WITH OBSERVATIONS

In recent decades, more than two hundred hot subdwarfs have been observed; ≈5 per cent of these have been identified as having helium-rich atmospheres (Ahmad & Jeffery 2003; Stroeer et al. 2007). In general, the helium-rich hot subdwarfs, including spectral types He-sdB and He-sdO, are divided into two groups: carbon-rich and nitrogen-rich. More than half of them show strong N II and N III lines in their optical spectrum; they are identified as nitrogen-rich by Drilling et al. (2003). The remainder show strong C II and C III lines and are labelled carbon-rich. The surface abundances of 33 He-sdO stars have been analysed in more detail by Hirsch (2009), while six He-sdBs are discussed by Naslim et al. (2010). These results are summarized in Table 1.

Table 1. Atmospheric parameters of He-sdO (Hirsch 2009) and He-sdB stars (Naslim et al. 2010). Helium, carbon and nitrogen abundances are given by mass fraction.

Star	$T_{\rm eff}$	log g	log $\beta_{\rm He}$	log$\beta_{\rm N}$	log $\beta_{\rm C}$	Sp type	CN-type
HE 0001−2443	39840	5.69	−0.002	−2.74	−4.52	He-sdO	N-rich
HE 0031−5607	39367	5.58	−0.002	−2.55	−4.52	He-sdO	N-rich
HE 0155−3710	40521	5.61	−0.002	−2.81	−4.52	He-sdO	N-rich
HE 0342−1702	41082	5.59	−0.004	−2.56	−4.51	He-sdO	N-rich
HE 1135−1134	40358	5.38	−0.107	−2.53	−4.31	He-sdO	N-rich
HE 1136−2504	41212	5.65	−0.097	−2.31	−4.32	He-sdO	N-rich
HE 1238−1745	38743	5.48	−0.272	−2.76	−4.14	He-sdO	N-rich
HE 1258+0113	39169	5.66	−0.237	−2.55	−4.17	He-sdO	N-rich
HE 1310−2733	40225	5.45	−0.105	−2.28	−4.31	He-sdO	N-rich
HE 1316−1834	41170	5.30	−0.003	−2.20	−4.52	He-sdO	N-rich
HE 1511−1103	41090	5.46	−0.008	−2.29	−4.33	He-sdO	N-rich
WD 0447+176	40545	5.54	−0.001	−2.71	−4.52	He-sdO	N-rich
WD 2204+071	40553	5.52	−0.078	−2.23	−4.36	He-sdO	N-rich
WD 2258+155	40619	5.71	−0.001	−2.76	−4.52	He-sdO	N-rich
HD 127493	42484	5.60	−0.027	−2.50	−4.46	He-sdO	N-rich
CD −31 4800	43080	5.87	−0.002	−2.50	−4.49	He-sdO	N-rich
CD −24 9052	41700	5.49	−0.195	−2.39	−4.21	He-sdO	N-rich
HE 1142−2311	51154	5.38	−0.016	−4.44	−1.70	He-sdO	C-rich
HE 1251+0159	45637	5.63	−0.010	−4.46	−1.72	He-sdO	C-rich
HE 1203−1048	44806	5.62	−0.009	−4.46	−1.71	He-sdO	C-rich
HE 0414−5429	43970	5.52	−0.005	−2.95	−2.04	He-sdO	C-rich
HE 0914−0341	45496	5.72	−0.004	−3.20	−2.26	He-sdO	C-rich
HE 0958−1151	44229	5.39	−0.011	−3.24	−1.64	He-sdO	C-rich
HE 1136−1641	43957	5.58	−0.006	−2.62	−2.05	He-sdO	C-rich
HE 1446−1058	45240	5.67	−0.013	−2.62	−1.60	He-sdO	C-rich
HE 2203−2210	47049	5.60	−0.009	−3.45	−1.72	He-sdO	C-rich
HE 2347−4130	45040	5.78	−0.002	−3.52	−2.40	He-sdO	C-rich
WD 2020−253	44105	5.51	−0.011	−2.68	−1.68	He-sdO	C-rich
HE 0952+0227	44266	5.45	−0.009	−3.08	−1.75	He-sdO	C-rich
UVO 0832−01	43953	5.66	−0.008	−2.77	−1.79	He-sdO	C-rich
UVO 0904−02	46170	5.64	−0.014	−3.60	−1.56	He-sdO	C-rich
HE 0016−3212	39186	5.13	−0.014	−2.29	−1.64	He-sdO	C-rich
HE 1256−2738	39571	5.66	−0.094	−2.44	−1.50	He-sdO	C-rich
LSB 1766	36340	5.19	−0.004	−2.71	−3.97	He-sdB	N-rich
SB 21	35960	5.40	−0.003	−2.76	−4.34	He-sdB	N-rich
BPS CS 29496−0010	39150	5.65	−0.002	−2.52	−4.19	He-sdB	N-rich
LB 3229	40000	5.15	−0.007	−2.34	−3.56	He-sdB	N-rich
BPS CS 22940−0009	33700	4.70	−0.007	−2.54	−2.13	He-sdB	C-rich
BPS CS 222956−0094	34280	5.63	−0.054	−2.58	−2.46	He-sdB	C-rich

5.1 Surface gravity–effective temperature diagram

In general, the double helium white dwarf merger represents an important evolution channel for the formation of helium-rich hot subdwarfs. Fig. 15 shows the evolutionary tracks for all four final masses (0.5, 0.6, 0.7 and 0.8 $M_\odot$) and all three model types (slow, fast and composite) on the surface gravity–effective temperature plane. In addition, the cases for a low-metallicity ($Z = 0.001$) compound model are also shown. In order to demonstrate the relation between helium white dwarf mergers and He-sdO stars, Fig. 16 shows the latter superimposed on an enlarged region of Fig. 15. The carbon abundance is represented by colour, while the abundance of nitrogen is represented by size. The splitting of the distribution is immediately apparent, for most carbon-rich stars are found at the hotter end of the distribution with $T_{\rm eff} \geq 43\,000$ K. Two exceptions, located in the cooler and carbon-poor population, also have a very high nitrogen abundance. With the exception of the low-metallicity ($Z = 0.001$) modes, the observed positions of helium-rich subdwarfs in the $T_{\rm eff}$–log (g) plane can be matched very well by the post-merger evolutionary tracks. The most carbon-rich stars are more likely to be associated with high-mass evolutionary tracks, possibly with $M > 0.6\,M_\odot$. For $Z = 0.001$ all evolutionary tracks crowd together at hotter temperatures; thus only the carbon-rich stars can match these tracks. There is no evidence to suggest that these stars have lower overall metallicities than the nitrogen-rich stars. In fact, quite the opposite is true, since surface nitrogen is representative of the sum of primordial carbon, nitrogen and oxygen converted to ^{14}N in the hydrogen-burning CNO cycle, which may thus be taken as a proxy for initial metallicity. The majority of He-sdOs have significant nitrogen abundances.

Fig. 17 shows the same information for the generally cooler He-sdB stars.[1] Four of these are carbon-poor and match the evolutionary

[1] The spectroscopic distinction between He-sdO and He-sdB is somewhat arbitrary. It depends primarily on the presence of He II absorption and the spectral resolution and signal-to-noise ratio at which the classification data were obtained. For convenience, we separate the groups analysed by Hirsch (2009) and Naslim et al. (2010).

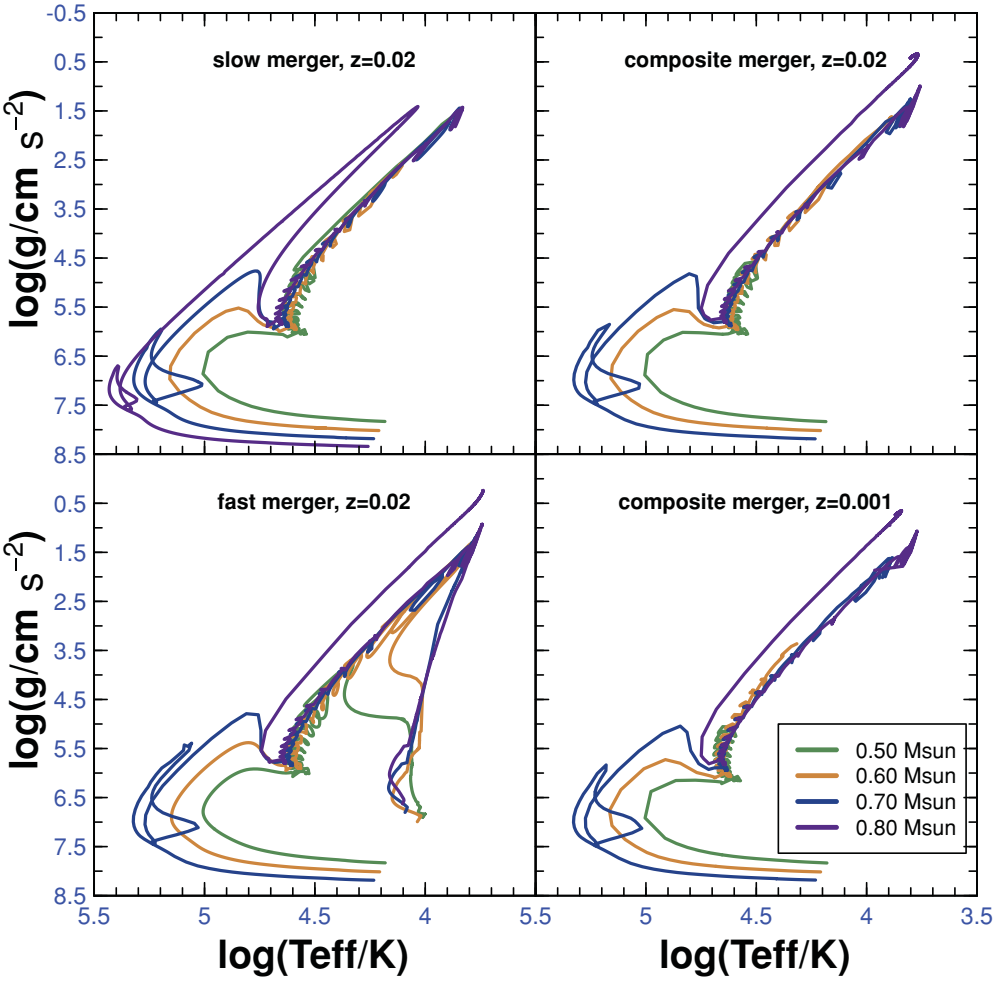

Figure 15. The evolutionary tracks of different masses on a gravity–temperature digram for each of the three models, i.e. slow, fast and composite merger. Additionally, a $Z = 0.001$ model of a composite merger is shown. The shading, from grey to dark, shows different masses in range 0.5–0.8 $M_\odot$.

tracks very well (Fig. 17). However, the remaining two stars are both carbon-rich and nitrogen-rich, and one is too cool to match any of the evolutionary tracks.

5.2 Surface abundances

Hirsch (2009) reports that 16 He-sdO stars are carbon-rich with abundances $-2.40 \leq \log \beta_C \leq -1.56$. 17 stars are carbon-poor with abundances $-4.52 \leq \log \beta_C \leq -4.14$, having a range of 0.38 dex, which is significantly narrower than for the carbon-rich case (0.84 dex). In addition, the nitrogen abundances lie in the range $-3.60 \leq \log \beta_N \leq -2.29$ for carbon-rich He-sdO (except three with $\log \beta_N < -4$) and in the range $-2.81 \leq \log \beta_C \leq -2.20$ for the carbon-poor case. Thus, nitrogen is more abundant in carbon-poor than in carbon-rich stars (Fig. 18).

For the slow merger model, all the products have the same surface abundance as the second helium white dwarf, i.e. $\log \beta_C = -4.19$ and $\log \beta_N = -1.89$. Thus, they are all nitrogen-rich stars. For the fast merger model, $\log \beta_C \approx -1.9$ but the nitrogen abundances are in the range $-3.9 > \log \beta_N > -11.0$, depending on mass. Thus, the fast merger model produces pure carbon-rich stars, with nitrogen likely to be unobservable (see Fig. 19). For the composite merger model, the surface abundances are divided into two groups by mass (Fig. 20). In general, models with final mass less than 0.7 $M_\odot$ will produce a nitrogen-rich star. Models with final mass greater than 0.7 $M_\odot$ will produce a carbon-rich star, but also retaining a significant nitrogen abundance. Thus, *most of the He-sdO and He-sdB stars can be explained by a double helium white dwarf merger, assuming that the accretion is divided into a fast coronal phase and a slow accretion phase.*

There are several exceptions, which may come from other channels. There are three He-sdO stars that are pure carbon-rich stars: HE 1142-2311, HE 1251+0159 and HE 1203-1048. It is possible that they come from a fast merger channel or from a merger in which the amount of material remaining in the disc is negligible. There are two He-sdO stars and two He-sdB stars (HE 0016-3212, HE 1256-2738, BPS CS 22940-0009 and BPS CS 222956-0094) that are are nitrogen-rich as well as carbon-rich. They are located near the low-mass evolution tracks. It is possible that these four stars come from a different evolution channel, for example the late

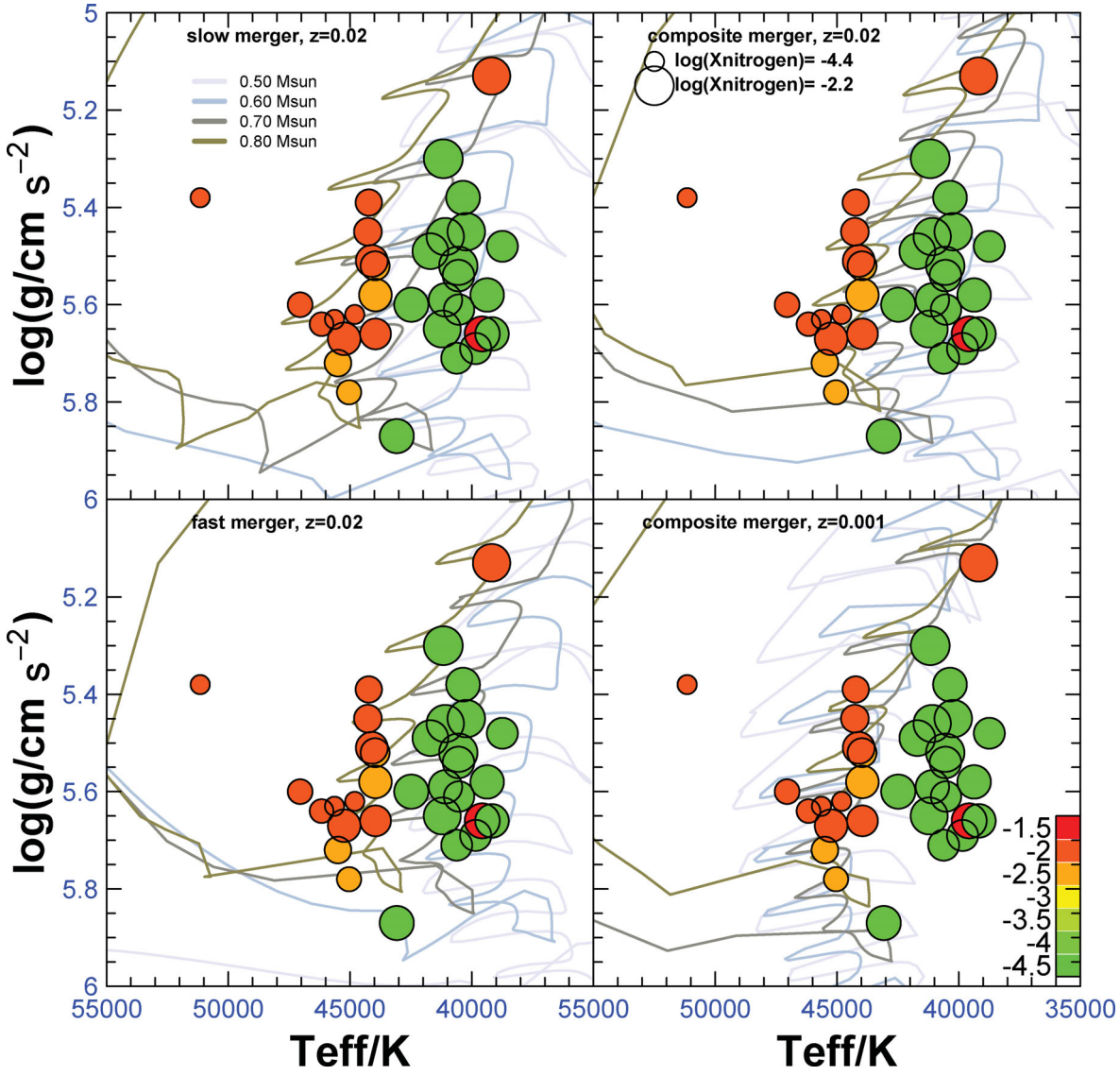

Figure 16. The evolutionary tracks of different masses on a gravity–temperature digram for each of the three models, i.e. slow, fast and composite merger. Additionally, a $Z = 0.001$ model of a composite merger is shown. The shading, from grey to dark, shows different masses in range 0.5–0.8 $M_{\odot}$. The coloured circle symbols shows the He-sdO from Hirsch (2009). The colour from light-grey (green online) to dark-grey (red online) shows the abundance of carbon in range −4.5 to −1.5 and the abundance of nitrogen is described by the size of the circle symbol.

helium-flash channel (Moehler et al. 2007; Miller Bertolami et al. 2008).

6 ADDITIONAL ABUNDANCE PREDICTIONS

In addition to ^{12}C and ^{14}N, surface abundances of the isotopes ^{13}C, ^{18}O and ^{22}Ne are also generated in our calculations. They show the different behaviour in different models.

6.1 ^{18}O and ^{22}Ne

As discussed above, the surface composition following a slow merger should be the same as the mean composition of the accreted white dwarf. In a fast merger, ^{18}O and ^{22}Ne are both enriched by α-captures on ^{14}N followed by extensive convective mixing. However, the composite merger model is slightly different: ^{18}O and ^{22}Ne are only enriched for final masses greater than 0.7 $M_{\odot}$ (Fig. 21).

6.2 ^{16}O/^{18}O and ^{12}C/^{13}C

In all of our models, the ^{13}C and ^{16}O abundances remained almost unchanged during the whole simulation. Thus, the ratio of ^{16}O/^{18}O and ^{12}C/^{13}C changed significantly due to the production of ^{12}C and ^{18}O. From the slow merger model to the fast merger model the ratio of ^{16}O/^{18}O decreases by a factor of about 1000, while the ^{12}C/^{13}C ratio increases by about 100. The results of the composite merger

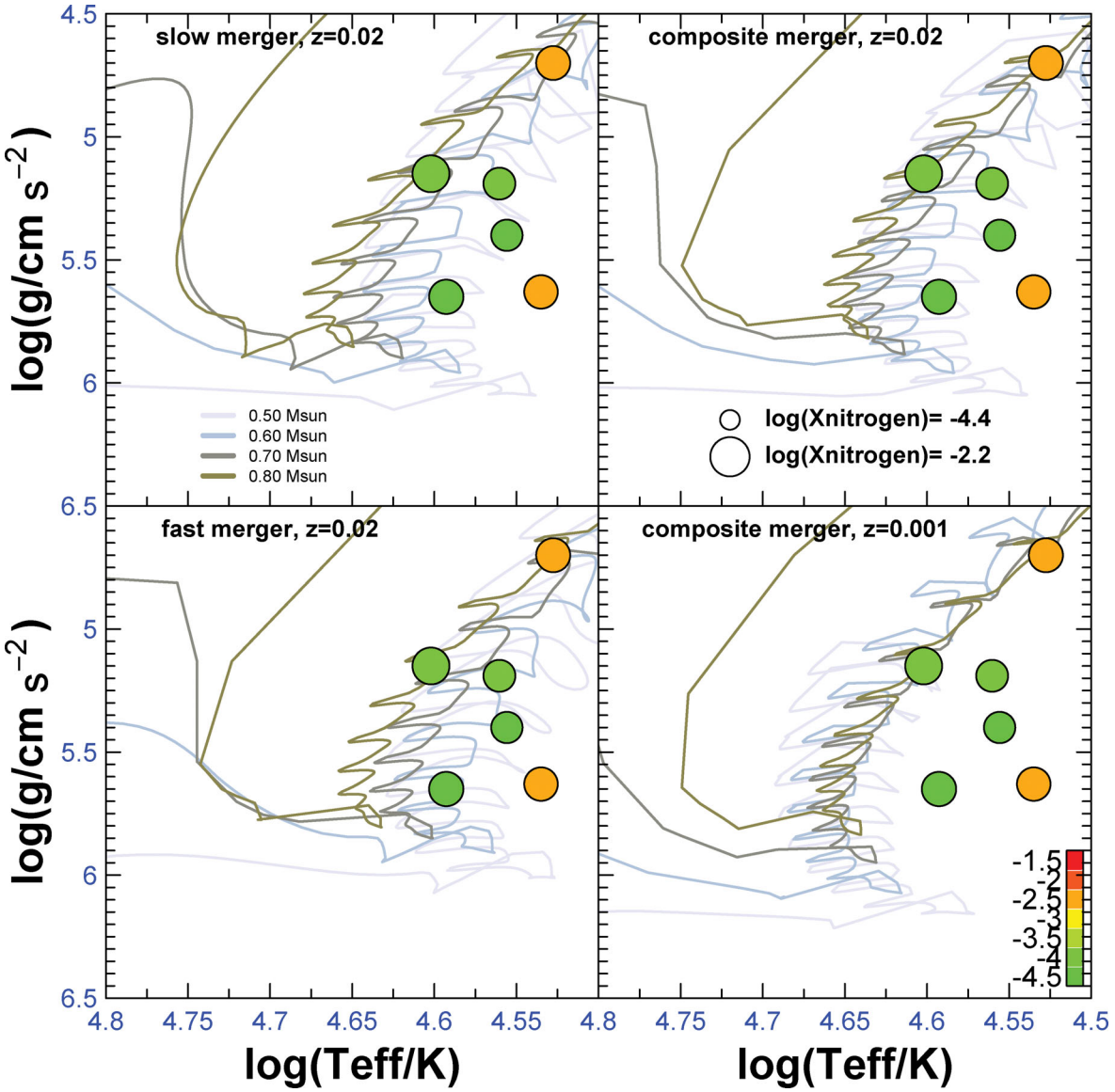

Figure 17. The evolutionary tracks of different masses on a gravity–temperature digram for each of the three models, i.e. slow, fast and composite merger. Additionally, a $Z = 0.001$ model of a composite merger is shown. The shading, from grey to dark, shows different masses in range 0.5–0.8 $M_{\odot}$. The coloured circle symbols shows the He-sdB from Naslim et al. (2010). The colour from light-grey (green online) to dark-grey (red online) shows the abundance of carbon in range −4.5 to −1.5 and the abundance of nitrogen is described by the size of the circle symbol.

simulations are slightly different and depend on the masses of the models (Fig. 22).

7 CONCLUSION

We have discussed three possible models for simulating the post-merger evolution of a helium + helium double white dwarf merger. These include slow (cold) accretion from a debris disc, fast (hot) accretion into a corona and a composite model involving both processes. Each model shows different initial evolution behaviour following the merger, although all end up evolving toward the helium main sequence through the g–$T_{\rm eff}$ domain populated by helium-rich hot subdwarfs.

All three models also show very different final surface abundances, particularly for carbon and nitrogen. In detail, the surface of the slow merger model retains the mean nitrogen-rich composition of the accreted white dwarf. The fast merger models possess a strong convection zone, which can dredge fresh carbon to the surface. The composite model retains elements of both slow and fast models. Thus, it produces nitrogen-rich surfaces for low-mass mergers, where the late accretion phases do not mix carbon-rich material into freshly accreted nitrogen-rich material. High-mass mergers on the other hand are predicted to have strong opacity-driven convection zones, which keep mixing this fresh material with carbon-rich layers beneath.

In the case of the composite model, there is a very convincing correlation between the position of carbon-rich He-sdOs and carbon-

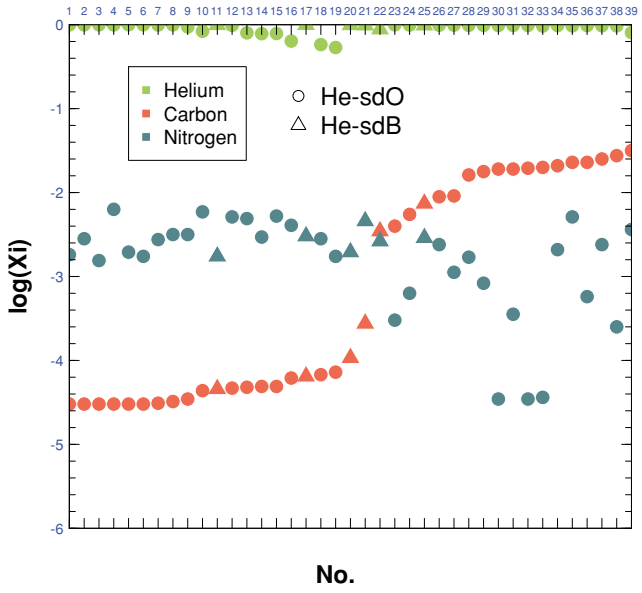

Figure 18. The distribution of surface abundance for He-sdO (Hirsch (2009), circles) and He-sdB stars (Naslim et al. (2010), triangles), ordered by carbon abundance. Elements are identifed by colour: light-grey (green online) for ^{4}He, mid-grey (red online) for ^{12}C and dark-grey (blue online) for ^{14}N.

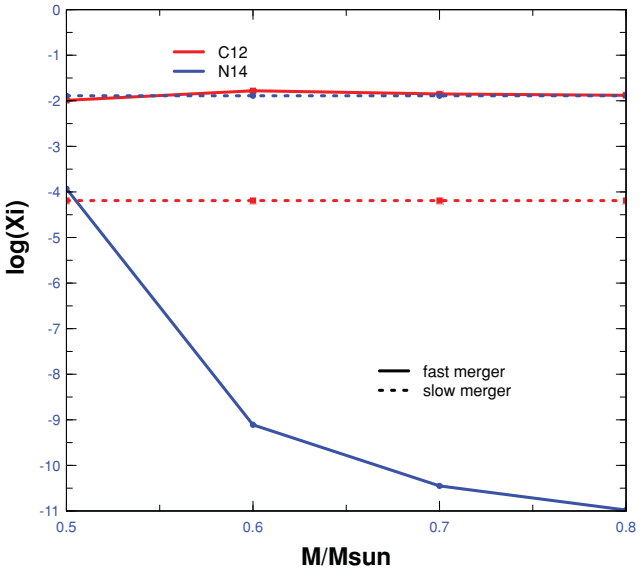

Figure 19. The surface abundance of slow (dotted) and fast (solid) merger models by mass. ^{12}C is shown by light grey (red in the online article), ^{14}N by dark grey (blue in the online article).

rich high-mass $M > 0.65\,\mathrm{M}_{\odot}$ evolution tracks, and between the position of nitrogen-rich He-sdOs and He-sdBs and nitrogen-rich low-mass $M < 0.65\,\mathrm{M}_{\odot}$ evolution tracks.

There are a number of assertions made in constructing the original model that allow for latitude in interpreting the detail of our results, including the choice of nearly equal mass components in the binary system and the choice of mass fraction apportioned to the corona and disc respectively in the composite model. These, as well as the

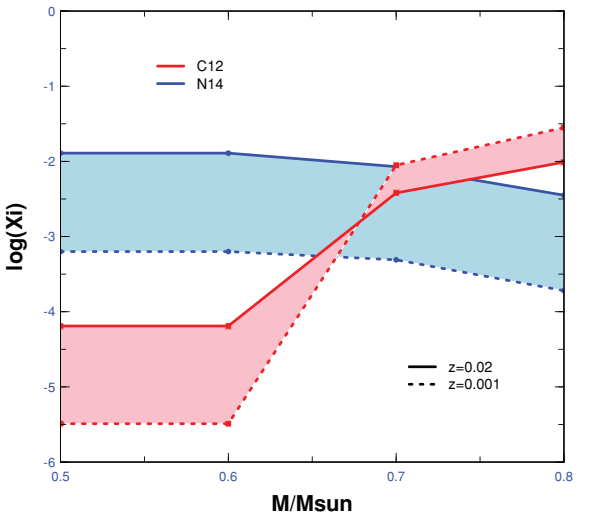

Figure 20. The surface abundance of the composite merger model by metallicity $Z = 0.02$ (solid) and $Z = 0.001$ (dotted). ^{12}C is shown by light grey (red in the online article), ^{14}N by dark grey (blue in the online article).

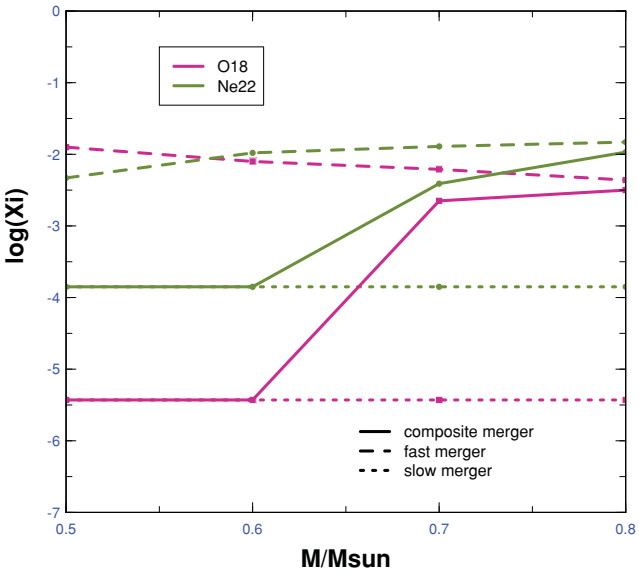

Figure 21. The surface abundance of ^{18}O (dark-grey, red online) and ^{22}Ne (light-grey, green online) in three different merger models: composite (solid), fast (dashed) and slow (dotted). All models are for $Z = 0.02$.

degree to which protons from the helium white dwarf atmospheres ingested into the corona lead to other interesting nucleosynthesis, must be examined in future investigations.

ACKNOWLEDGMENTS

We thank the anonymous referee for helpful comments. The Armagh Observatory is supported by a grant from the Northern Ireland Department of Culture Arts and Leisure. XZ thanks Dr P. Lorén-Aguilar for kindly offering simulation data of the white dwarf merger process. XZ also thanks Bill Paxton for his help with MESA.

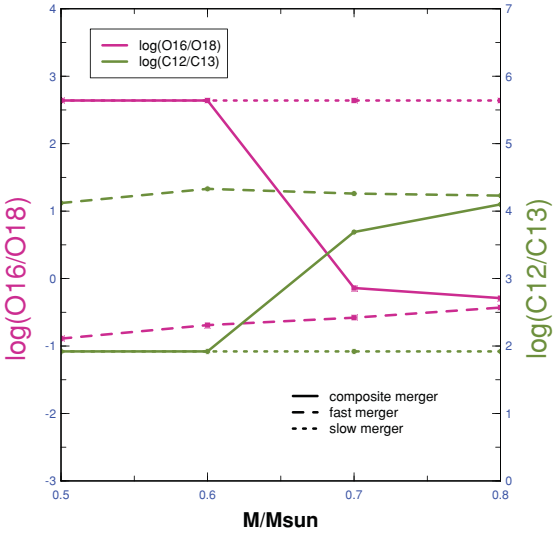

Figure 22. The surface abundance of $\log(^{16}O/^{18}O)$ (dark-grey, red online) and $\log(^{12}C/^{13}C)$ (light-grey, green online) in three different merger models: composite (solid), fast (dashed) and slow (dotted). All models are for $Z = 0.02$.

REFERENCES

Ahmad A., Jeffery C. S., 2003, A&A, 402, 335
Alexander D. R., Ferguson J. W., 1994, ApJ, 437, 879
Benz W., Cameron A. G. W., Press W. H., Bowers R. L., 1990, ApJ, 348, 647
Brown J. M., Kilic M., Brown W. R., Kenyon S. J., 2011, ApJ, 730, 67
Clayton G. C., Geballe T. R., Herwig F., Fryer C., Asplund M., 2007, ApJ, 662, 1220
Drilling J. S., Moehler S., Jeffery C. S., Heber U., Napiwotzki R., 2003, in Gray R. O., Corbally C. J., Philip A. G. D., eds, The Garrison Festschrift Spectral Classification of Hot Subdwarfs. Univ. Arizona Press, Tucson, p. 27
Green R. F., Schmidt M., Liebert J., 1986, ApJS, 61, 305
Guerrero J., García-Berro E., Isern J., 2004, A&A, 413, 257
Han Z., 2008, A&A, 484, L31
Han Z., Podsiadlowski P., Maxted P. F. L., Marsh T. R., Ivanova N., 2002, MNRAS, 336, 449
Han Z., Podsiadlowski P., Maxted P. F. L., Marsh T. R., 2003, MNRAS, 341, 669
Heber U., 2009, ARA&A, 47, 211
Heber U., Kudritzki R. P., Caloi V., Castellani V., Danziger J., 1986, A&A, 162, 171
Hirsch H., 2009, PhD thesis, University of Erlangen-Nürnberg
Iben I., Jr, Tutukov A. V., 1984, ApJS, 54, 335
Iglesias C. A., Rogers F. J., 1996, ApJ, 464, 943
Jeffery C. S., Drilling J. S., Harrison P. M., Heber U., Moehler S., 1997, A&AS, 125, 501
Justham S., Podsiadlowski P., Han Z., 2011, MNRAS, 410, 984
Kilic M., Brown W. R., Allende Prieto C., Kenyon S. J., Panei J. A., 2010, ApJ, 716, 122
Kilic M., Brown W. R., Allende Prieto C., Agüeros M. A., Heinke C., Kenyon S. J., 2011, ApJ, 727, 3
Landau L., Lifshitz E., 1962, in The classical theory of fields. Pergamon, Oxford, pp 1–352
Lorén-Aguilar P., Isern J., García-Berro E., 2009, A&A, 500, 1193
Lynden Bell D., Pringle J. E., 1974, MNRAS, 168, 603
Miller Bertolami M. M., Althaus L. G., Unglaub K., Weiss A., 2008, A&A, 491, 253
Mochkovitch R., Livio M., 1989, A&A, 209, 111
Mochkovitch R., Livio M., 1990, A&A, 236, 378
Moehler S., Richtler T., de Boer K. S., Dettmar R. J., Heber U., 1990, A&AS, 86, 53
Moehler S., Dreizler S., Lanz T., Bono G., Sweigart A. V., Calamida A., Monelli M., Nonino M., 2007, A&A, 475, L5
Naslim N., Jeffery C. S., Ahmad A., Behara N. T., Şahìn T., 2010, MNRAS, 409, 582
Nelemans G., Verbunt F., Yungelson L. R., Portegies Zwart S. F., 2000, A&A, 360, 1011
Nomoto K., Iben I., Jr, 1985, ApJ, 297, 531
Paxton B., Bildsten L., Dotter A., Herwig F., Lesaffre P., Timmes F., 2011, ApJS, 192, 3
Rebassa-Mansergas A., Nebot Gómez-Morán A., Schreiber M. R., Girven J., Gänsicke B. T., 2011, MNRAS, 413, 1121
Saio H., Jeffery C. S., 2000, MNRAS, 313, 671
Saio H., Jeffery C. S., 2002, MNRAS, 333, 121
Saio H., Nomoto K., 1998, ApJ, 500, 388
Stroeer A., Heber U., Lisker T., Napiwotzki R., Dreizler S., Christlieb N., Reimers D., 2007, A&A, 462, 269
Tutukov A., Yungelson L. R., 1979, Acta Astron., 29, 665
Warner B., 1967, MNRAS, 137, 119
Yoon S., Podsiadlowski P., Rosswog S., 2007, MNRAS, 380, 933

This paper has been typeset from a TEX/LATEX file prepared by the author.